https://doi.org/10.1016/j.electacta.2019.03.016

RGB Video electrochemistry of copper electrodeposition/electrodissolution in acid media on a ternary graphite:copper:polypropylene composite electrode

J. Agrisuelas, J.J. García-Jareño[*]*, E. Guillén, F. Vicente*

Department of Physical-Chemistry, University of Valencia.

Dr. Moliner 50, 46100 Burjassot (Spain)

* To whom correspondence should be addressed Jose.J.Garcia@uv.es

Abstract

Galvanostatic copper electrodeposition and electrodissolution on graphite:copper:polypropylene composite electrodes in acidic media have been investigated to extend the technological applicability of ternary composites. Both electrochemical processes were monitored by RGB video electrochemistry. The analysis of digital images allowed the color changes on the electrode surface to be investigated. We estimate the growth rate of the copper layer in two different electrode geometries. The relatively high resistance of this composite causes a gradient of the electric resistance along the electrode involving a non-homogeneous electrodeposit growth in $CuSO_4/H_2SO_4$ aqueous solutions. Copper electrodissolution was studied in HCl and H_2SO_4 aqueous solutions. Whereas chloride anions stabilized cuprous cation, the electrodissolution process in HCl takes place apparently by a more complicated mechanism. Dispersion of color estimated from the standard deviation of the RGB color images was also analyzed and it has been postulated as a tool for identifying possible intermediate species on the electrode surface.

1 INTRODUCTION

Polymer-based composite materials have been the subject of many research works due to their low weight, low cost and easy processability [1–6]. The electrical properties of composites can be tuned by the dispersion of metallic particles into the polymeric matrix, but it can turn this material fragile and heavy [7–9]. Conductive fillers based on carbonaceous micro or nanoparticles overcomes both issues due to their low density [10–12]. However, carbonaceous-based composites present a high electrical resistance making difficult their use in some cases if compared with binary metal:polymer composites [7,12,13]. Ternary graphite:metal:polymer composites reduce the electrical resistance and represent an interesting solution to be used as electrodes in different technological devices [14].

We study electrodeposition and electrodissolution of Cu on the surface of ternary graphite:metal:polymer composites. These processes will be affected by the ohmic drop along the electrode. In resistive electrodes, the electrical resistance (R_E) along the electrode (**Figure S1**) changes gradually as:

$$R_E = \rho \cdot \frac{x}{S} \quad (1)$$

where ρ is the electrode resistivity, S the electrode section area and x is the distance between the electrical contact at x = 0 (top) and any point along the electrode limited by the electrode length at $x = L$ (bottom). The effect of the ohmic drop proves more evident if the electrical resistance and/or current increase [15–21]. If ρ and S keep constant along the electrode, R_E changes linearly from x = 0 to $x = L$. Thus, the potential gradient along the electrode ($E(x)$) due to the ohmic drop can be expressed as [16,18,19,22]:

$$E(x) = E_{app} - i \cdot R_E = E_{app} - i \cdot \rho \cdot \frac{x}{S} \quad (2)$$

where E_{app} is the applied potential and i the current. If R_E or i are 0, then, $E(x) = E_{app}$ anywhere on the electrode surface. On the contrary, if $i \cdot R_E$ reaches high values, the potential is not homogeneous along the electrode causing a gradient in the extension of electrochemical processes [7,17–19]. In fact, the ohmic drop leads to misinterpretations of experimental data: e.g. the voltammetry waves distortions has been attributed to other processes such as diffusion [18] or explained as constant phase elements (CPE) in impedance measurements [9,13].

In this context, we expect the that ohmic drop causes an inhomogeneous deposit of electroactive materials (conducting polymers or metals) along the electrode surface. A large amount of electrodeposited material would be found close to the electrical contact ($x = 0$) since there is the smallest resistance. Similarly, electrodissolution would take place fastest at these zones.

Electrodeposition depends on the nature of the electrode material but also on the geometry of the electrode. If the electrodeposition mechanisms on composites are understood, we can extend their technological applicability as occurs in other materials [23]. For example, copper metal electrodes could be substituted by low-cost and lightweight catalyst electrodes of copper-covered ternary composites [24–27].

Copper electrodeposition in $CuSO_4/H_2SO_4$ aqueous solutions has proved a high yield electrodeposition process apparently without the participation of intermediates [28–30]:

$$Cu^{2+} + 2e^- \xrightarrow{k} Cu \qquad (3)$$

Likewise, the electrodissolution in diluted H_2SO_4 solutions is apparently similar at high electrodissolution rates [28,31,32]. On the contrary, chlorides of HCl solutions stabilize some intermediate copper species and the electrodissolution should be described as a more complex process including at least two single electron transfers [33–37]:

$$Cu \xrightarrow{k_1} Cu^+_{ads} + e^- \qquad (4)$$

$$Cu_{ads}^{+} \xrightarrow{k_2} Cu_{ads}^{2+} + e^{-} \text{ (slow)} \quad (5)$$

$$Cu_{ads}^{2+} \xrightarrow{k_3} Cu_{aq}^{2+} \quad (6)$$

Electrodeposition or electrodissolution of copper on an electrode involves color changes at the electrode|solution interface. These color changes can be studied by spectroscopy techniques. However, carbonaceous-based composites are opaque, with a characteristic black color and a rough surface what prevents good reflectance measurements [38]. In addition, the response obtained by spectroscopy techniques corresponds to a small region of the electrode surface [39–41]. Considering that composite electrode surfaces could not be homogeneous, this fact would involve repetitive spectroscopic measurements at different zones to map the surface. On the contrary, the surface analysis using digital images provides information about the complete electrode surface with a good resolution [38,42]. This optical technique has been used for the color analysis of pictures in different topics as the characterization of fruits [43], colorimetric sensors [44,45] or solar cells [46].

Vidal et al. used a similar technique for the analysis of electroplated surfaces [47]. The color analysis from digital images acquired with a flatbed scanner of metallic electrodeposits provides accurate information of plated quality. The images were decomposed to the RGB model and allowed obtaining analytical information after deposition of Ni in different experimental conditions. The standard deviation has been related with the quality of the final plated surface. In our case, digital images were obtained simultaneously during the electrochemical processes by recording digital video and providing in situ information about the pixel color evolution at any point on the electrode surface and also at any time. Therefore, we can also analyze the time evolution of standard deviation and mean color intensities and not only the final quality. In view of the promising results obtained for the Cu electrodissolution on opaque composite electrodes using the analysis of RGB digital videos [38], the aim of this work is to extend the study about the electrochemical deposition and dissolution of copper in

acidic media on a ternary graphite:copper:polypropylene composite electrode and the resistivity effects on the rate of the electrochemical processes at the electrode|solution interface along the electrode. Cu electrodeposits were obtained from solutions of $CuSO_4/H_2SO_4$ and the copper electrodissolution was studied in H_2SO_4 and HCl aqueous solutions. In order to study the ohmic drop effect, two electrode geometries were tested, a short electrode (1.1 cm x 0.5 cm x 0.2 cm) and a long electrode (2.5 cm x 0.5 cm x 0.2 cm).

2 EXPERIMENTAL

2.1 Apparatus

Electrochemical experiments were performed with a PAR 273A potentiostat/galvanostat. The working electrode was a composite electrode composed by graphite and copper powder randomly dispersed into a polypropylene matrix (CCuPP, 40:10:50 in weight) or a metallic Pt disc (1 cm^2). Short (1.1 cm x 0.5 cm x 0.2 cm) and long (2.5 cm x 0.5 cm x 0.2 cm) composite electrodes were accurately disposed in the electrochemical cell to obtain comparable values. A platinum mesh was the counter electrode and no inert atmosphere was used. The electrochemical cell was a 5 cm x 2 cm x 2 cm high-transmittance glass cell (Hellma, OG quality). Digital endoscope camera (EPA-503278) with USB connection was used to capture 640×480 color digital videos at 30 frames per second (fps). The electrochemical cell was illuminated in a homemade white box with a T5 6400K fluorescent tri-phosphor lamp (color rendering index 80) under controlled conditions and the acquisition parameters of the digital camera such as exposition, white balance and frame rate were kept constant.

2.2 Electrode surface modifications

Copper was deposited by chronopotentiometry by applying −8 mA in 0.5 M $CuSO_4$ (Scharlau) and 0.1 M H_2SO_4 (Fisher scientific) and was dissolved in 0.1 M H_2SO_4 or in 0.1 M HCl (Scharlau) solutions by applying 8 mA. Deposition and dissolution times were 4000 s for

the CCuPP and 400 s for the Pt disc electrode. All reagents were analytical grade, used as received and dissolved in Milli-Q-plus H_2O (resistivity 18.2 MΩ cm).

2.3 Image processing

Digital full-colored videos acquired at 30 fps and synchronized with the electrochemical experiments were separated into jpg format images. The sequentially extracted images were read using Mathcad® v14 routines. After selecting the region of interest, all cropped images were automatically decomposed into the red (R), green (G) and blue (B) color matrix. The pixel intensities of the RGB matrix vary between 0 and 255 (8 bits). We calculate mean intensity values ($\bar{I}$) and the associated standard deviation (sd) for each color matrix and at each region under study by:

$$\bar{I}_{R,G\ or\ B} = \left(\sum_{i=1}^{n_{pixel}} \frac{I_i}{n_{pixel}} \right) \tag{7}$$

$$sd_{R,G\ or\ B} = \sqrt{\sum_{i=1}^{n_{pixel}} \frac{(I_i - \bar{I})^2}{n_{pixel} - 1}} \tag{8}$$

where n_{pixel} is the total number of pixels in the cropped image. On the one hand, $\overline{I_i}$ values near 0 indicate absence of color light or in other words black color whereas $\bar{I}_i$ values near 255 mean the corresponding pure color (R, G or B). On the other hand, sd reveals the color homogeneity of the analyzed spatial region . Relatively lower sd values correspond to more homogeneous colored surfaces and relatively higher sd values to heterogeneous color surface[47]. In addition, the plot of *sd* against the elapsed time during the transition between two homogeneous colors show a peak where the maximum value corresponds to the half-transition point [48].

3 RESULTS AND DISCUSSION

3.1 Copper electrodeposition

After Cu electrodeposition on the composite electrode, the surface color changed from graphite color (RGB coordinates: 14;6;14) to the copper color (227;160;123) in the air. However, in the $CuSO_4/H_2SO_4$ aqueous solution, RGB coordinates of CCuPP changed from (6;40;49) to (46;169;206) due to the characteristic blue color of the $Cu(H_2O)_6^{2+}$ complex that masks $\bar{I}_R$ changes. Accordingly, we focused our interest on the $\bar{I}_G$ changes to analyze the copper electrodeposition process on CCuPP since blue changes can also be affected by the solution color.

<**Figure 1**>

Figure 1 shows the 3D surface contour map of the mean green intensity ($\bar{I}_G$) against the elapsed time and the distance from the electric contact for both electrode geometries. As expected, Cu electrodeposited faster on the top of the CCuPP electrode due to the lowest R_E at this zone. For the short electrode, $\bar{I}_G$ shows a smooth and regular change during the electrodeposition. We assumed Eq. (3) governs the Cu electrodeposition since apparently no different compounds (colored species) appeared on the electrode surface [28]. Remarkably, we observed a significant accumulation of Cu at the bottom of CCuPP due to the accumulation of electrical charges and the easy transport of electroactive species around the sharp edges of electrodes [49]. After electrodeposition, the short electrode showed a more homogeneous coated surface, while for the long one, the electrode seemed slightly coated beyond 1.2 cm after 4000 s.

<**Figure 2**>

At this point, one limitation of digital image analysis in this system is that it is not possible to distinguish between deposits with different thickness since they would show the

same RGB coordinates for the copper color. However, the evolution of the CCuPP coating fraction (θ in %) can be estimated as:

$$\theta = 100 \cdot \left(\frac{\bar{I}_G - \bar{I}_{G,0}}{\bar{I}_{G,MAX} - \bar{I}_{G,0}} \right) \quad (9)$$

considering that any zone on the electrode surface immersed in the $CuSO_4/H_2SO_4$ aqueous solution could show two possible colors: the color for the non-covered CCuPP surface corresponding to the green intensity before the electrodeposition ($\bar{I}_{G,0} = 32$) and copper color after electrodeposition ($\bar{I}_{G,MAX} = 178$).

Figure 2 shows that the copper layer grew up faster initially on the top due to the lower R_E in both electrode geometries. For the short electrode (**Figure 2A**), Cu coated the top region after 1000 s, and after 2000 s, the surface electrode was completely coated and a stable potential around –2.4 V was reached (inset of **Figure 2A**). The stable potential reveals when the whole electrode surface was coated by at least one continuous copper layer eliminating the intrinsic CCuPP ohmic drop. Considering a similar deposited mass on both electrodes since the applied charge was the same, no region reached a 100 % coating for the long one (**Figure 2B**). The bottom was uncoated after 4000 s (around 20% at 2.3 cm) due to the preference of Cu deposition on the continuous Cu layer formed on top. Current flowed easier through this conducting layer with a metallic resistance ($R_E \approx 0\ \Omega$) than on CCuPP (scheme in **Figure 2C**). Consequently, the long electrode never reached a stable potential during the electrodeposition time (inset of **Figure 2A**).

Additionally, we can calculate the growth rate in terms of coating fraction at different parts on the electrode surface from the slope of θ_G against time between 0 and 200 s (**Figure 2**). This allows us a quantitative approach of the Cu electrodeposition depending on the electrode geometry. For the long one, we estimated growth rates of 0.090 % s^{-1}, 0.016 % s^{-1}, 0.012 % s^{-1} and 0.007 % s^{-1} in four discrete points from the top to the bottom. Comparing the

top and bottom values, the growth rate decreased close to 14 times mainly due to the ohmic drop effect. For the short one, the growth rates proved 4-5 times faster going from 0.38 % s^{-1} at the top to 0.11 % s^{-1} at the bottom. As can be seen, a small increment in length of 1.4 cm significantly affects the coating process in resistive electrodes such as CCuPP composites.

<Figure 3>

To compare, we repeated the same electrodeposition experiment on a Pt disc conductive electrode. As expected, the color of the metallic electrode changed homogeneously on all the disc surface. During the deposition, we observed that most of the Pt surface was coated by Cu in less than 100 s (**Figure 3A**). In this time interval, we observed a standard deviation (sd_G) peak at 26 s (**Figure 3B**) which means that the Cu layer coated half of the Pt surface as demonstrated below. After this time, $\bar{I}_G$ changes slowly and sd_G decreased since the electrodeposition homogenized the surface color.

As proved in previous works, the analysis of sd provides interesting information about the homogeneity of the electrode surface [47,48]. Let us suppose that each point on the composite surface can be only Cu color (*C*) or CCuPP black color (*B*). So, we can rewrite Eq (8) as:

$$sd = \sqrt{\frac{n_C\left(I_C - \bar{I}\right)^2 + n_B\left(I_B - \bar{I}\right)^2}{n_T - 1}} \tag{10}$$

where

$$\bar{I} = \frac{n_C I_C + n_B I_B}{n_T} \tag{11}$$

n_i represents the number of pixels with color C or B, and $n_T = n_C + n_B$ is the total number of analyzed pixels. Differentiating Eq. (10) and equaling to zero, we obtain the maximum value of sd when

$$n_C = \frac{1}{2} n_T = n_B \quad (12)$$

This maximum could be interpreted as a characteristic half-life time ($t_{1/2}$) [48].

If θ growths linearly, the sd evolution appears as a symmetrical peak but if the growth rate decreases exponentially, then sd evolution appears as a non-symmetrical peak (see supplementary material). The latter was observed during Cu deposition on Pt electrode (**Figure 3B**). The lowest sd is reached when the whole surface has the same color: Pt color or Cu color. During the electrodeposition process at constant current, the coated region by Cu is larger each time but θ growths slower since there is no color change if Cu deposited on Cu. This caused the asymmetry of experimental sd peaks.

Figure 4 shows sd_G evolution of 0.1 cm (long) x 0.5 cm (width) rectangular regions along the electrode surface during the electrodeposition. For the short geometry, sd_G peaks displaced to larger times and appeared wider for longer distances from the top. The asymmetry of sd_G peaks reflects the non-constant Cu growth rate which, at the same time, depends on the distance from the top of the electrode (**Figure 4A**). For the longest electrode and for the longest distances (**Figure 4B**), sd_G increased continuously without a peak configuration when the distances were longer than 1.5 cm. In addition, sd_G did not reach the minimum for distances longer than 0.2 cm because the complete coating process took place only close to the top of the electrode.

<**Figure 4**>

Estimated values of $t_{1/2}$ obtained from sd_G peaks were plotted at different distances for both geometries (inset of **Figure 4A**). As expected, larger $t_{1/2}$ were obtained for the long electrode. In both geometries, we observed an exponential dependence of $t_{1/2}$ on the distance from the top of electrode. The growth rate could be exponentially dependent on the effective potential based on a Butler-Volmer kinetic model. This fact agrees with the ohmic drop effect

since resistance changes linearly with the distance from the top of the electrode and therefore the effective potential on the electrode surface also (Eq (2)).

3.2 Copper electrodissolution

Cu electrodeposited on both CCuPP geometries was electrodissolved in 0.5 M H_2SO_4 and in 0.5 HCl. As both solutions are transparent, we could analyze $\bar{I}_R$ since showed the highest change against time and the best resolution. During the discussion of the electrodissolution results, we should keep in mind that Cu layer thickness deposited on both CCuPP geometries was not constant along the electrode surfaces according to the above results.

3.2.1 H_2SO_4 aqueous solution

Figure 5 shows how θ_R decreases during the electrodissolution process in H_2SO_4 aqueous solutions for both electrodes to return to the RGB color values for a bare CCuPP. Comparing θ_R changes for both geometries, one can see small differences between the top and the bottom for the short one due to the more homogeneous thickness of the deposited Cu layer. Particularly during the first 250 s, we appreciated that the electrode surface appeared slightly darker and, consequently, $\bar{I}_R$ and θ_R decreased. We attributed this fact to the formation of insoluble Cu_2O (red), CuOH with impurities (dark red) and/or CuO (black) compounds [50–54] accelerated by the O_2 reduction [55].

Figure 5 shows also the dependence of measured potential against the elapsed time. For both geometries, continuous and small potential changes appeared until 3000-3500 s followed by an abrupt potential increase to around 3 V with the subsequent formation of bubbles. After the Cu exhaustion on the electrode surface, the current passing through the electrochemical cell caused the oxidation of the media solution. The largest bubbles appeared on the top where R_E proved the smallest one (**Figure 5A**).

<**Figure 5**>

For the short electrode (**Figure 5A**), θ_R profiles are very similar independently of the distance from the top of the electrode. On the contrary (**Figure 5B**), Cu layer at the bottom was completely dissolved at around 3200 s for the long electrode but the top of this electrode needed almost 3800 s. For the top, Cu electrodissolution takes place mostly on the outer Cu metal surface and, therefore, the θ_R changes slowly. In both cases, when the last Cu metal on the CCuPP surface disappears the mean color intensity ($\overline{I_R}$) and θ_R change abruptly near 3800 s (**Figure 5**). Considering 4000 s of electrodeposition, we can estimate an electrodeposition yield of about 95% (3800/4000).

The evolution of sd_R against the elapsed time in **Figure 6** shows different peaks. As above mentioned, each peak means the transition between two different color surfaces which could be associated with the formation of new adsorbed species formed during the Cu electrodissolution in non-deaerated solutions. For the short electrode, sd_R shows a first peak around 250 s ($t_{1/2}$) (**Figure 6A**). According to Eq. (12), one half of the metallic Cu layer is covered by darker species (Cu_2O, CuOH and/or CuO) at this time. Between 2800 s and 3600 s and depending on the distance from the top, we observe new sd_R peaks appearing first at long distances which were wider than those corresponding to zones near the top of the electrode. These peaks were associated with the transition between the Cu layer on the electrode surface and the naked electrode. This fact can be easily explained since there is a smaller amount of Cu deposited at larger distances from the top of the electrode. The last region to be electrodissolved shows the thinnest peaks corresponding to the top of the electrode where the electrochemical reaction took place faster.

For the longer electrode (**Figure 6B**), sd_R profiles were different but the electrodissolution mechanism was similar. At the largest distances from the top, we did not observe sd_R peaks since less than half of the CCuPP surface was covered by Cu (around 20% as indicated in **Figure 6B**). For intermediate distances, a peak appeared when the Cu layer

coated half of the electrode surface. However, a double peak appears at the top of the electrode. The first and wide peak could be associated with the formation of dark species coating half of the Cu surface. The narrow peaks could be associated with the dissolution of the last Cu layer on the electrode.

After Cu electrodissolution (from 3800 s), there was a significant sd_R increase in both geometries due to the formation of bubbles on the naked CCuPP surface. It should be noted that these bubbles are better detected by sd_R (**Figure 6**) changes than by $\bar{I}_R$ or θ_R (**Figure 5).**

3.2.2 HCl aqueous solution

<**Figure 7**>

In 0.1 M HCl solution, the initial darkening of the Cu layer surface proves more evident than in H_2SO_4 during the first 200 s (**Figure 7A**). Concerning the nature of this layer, CuCl, Cu_2O, $Cu_2(OH)_3Cl$ and $Cu(OH)_2$ layers on the electrode surface have been postulated during Cu corrosion in HCl media [56–60]. After that, the electrode surface color was clearer ($\bar{I}_R$ increased) and changed slowly until near 3800 s.

At around 3500 s, a white/grey layer appeared on the electrode surface. Some authors proposed the formation of CuCl species in low chloride concentrations [59,61,62] and CuCl salt color coincides with this layer color [63]. After a few seconds, this layer disappeared, and the characteristic black color of the CCuPP surface was visible (**Figure 7A**).

After the complete Cu electrodissolution, bubbles (preferably observed on the top of the electrode where R_E proves the smallest) appeared on the CCuPP surface also accompanied by an abrupt increase of the measured potential indicating that a different faradaic process occurred (**Figure 7A**). We attribute these bubbles to the Cl^- insertion and oxidation to Cl_2 since the potential measured during the bubble formation in HCl (2.8 V) was lower than this one in H_2SO_4 solution (3.2 V).

Figure 7B shows several sd_R peaks during Cu electrodissolution evolution in HCl solutions. The first peak appears during the first 200 s due to a dark red layer formation on the Cu surface. Next, the dark layer disappeared and sd_R showed a new peak at 750 s. About 2800 s, the dissolution of the last Cu layer and the formation of the white/grey CuCl layer occurred. At 3750 s, the white/grey layer covers one half of the black CCuPP surface. Finally, the last sd_R peak corresponds to the gas bubbles generation on the CCuPP surface. These sd_R peaks allow us to find out the complexity of the surface mechanisms on an electrode.

To assure the nature of the white/grey $CuCl_{ads}$ layer and the proposed mechanism two experiments were performed. First, the Cu layer on a Pt disk electrode was electrodissolved in similar conditions. As in CCuPP, the Cu surface initially changed to a dark and reddish color (see supplementary material) and, again, a white layer appeared on the surface which disappeared after a few seconds at the end of the experiment. Then, the bright Pt surface became completely visible. In this case, the color change was less evident than for the CCuPP electrode since the white/grey CuCl layer and the Pt surface have similar colors. This evidence allows us to discard the intrinsic characteristic of the CCuPP electrode as responsible for the CuCl formation. Therefore, we could attribute this fact to the environmental conditions on the electrode surface. Second, we analyzed a CCuPP electrode removed from the HCl solution during the CuCl formation by EDAX microanalysis (**Figure 8**). We can observe in this Figure two different regions, the black one corresponds to the naked composite surface and the white one corresponds to the new layer formed on the electrode surface during the electrodissolution. The results confirmed that this layer contains almost 50% of Cu and 50% of Cl, therefore CuCl is the most plausible composition of this layer (**Figure 8**).

3.2.2 Proposed Cu electrodissolution mechanism in aerated HCl aqueous solution

Larsen et *al* proposed the following Cu corrosion mechanism in HCl [60]:

$$Cu + 2Cl^- \rightleftarrows CuCl_{2\,ads}^- + e^- \quad (13)$$

$$CuCl_{2\,ads}^- \rightarrow CuCl_{2\,sol}^- \quad (14)$$

and for the oxide formation:

$$2CuCl_{2\,ads}^- + H_2O \rightarrow Cu_2O_{ads} + 2H^+ + 4Cl^- \quad (15)$$

$$Cu_2O_{ads} + 2H^+ + 4Cl^- \rightarrow 2CuCl_{2\,sol}^- + H_2O \quad (16)$$

In this mechanism, Cu dissolves as Cu(I). In our case, theoretically, only about 2000 s should be necessary to complete the Cu electrodissolution. However, the electrodissolution process took about 3700 s to be completed applying 8 mA. On the one hand, we can assume that Cu dissolved mostly as Cu(II) like in H_2SO_4. On the other hand, a small part of Cu passed to the solution by a chemical attack or as Cu(I) species stabilized by the presence of Cl^- anions. Thus, we propose the following Cu electrodissolution mechanism in aerated 0.1 M HCl solutions:

$$Cu \rightarrow Cu_{ads}^+(\text{stabilized by } Cl^-) + e^- \quad (17)$$

$$2Cu_{ads}^+ + 2H_2O \rightarrow Cu_2O_{ads} + H_3O^+ \quad (18)$$

$$Cu_2O_{ads} + H_3O^+ \rightarrow Cu_{aq}^{2+} + 2H_2O + e^- \quad (19)$$

For the last layer, after Cu was completely removed from the electrode surface, there was an approach of Cl^- anions to the electrode surface favoring the oxidation of Cl^- to Cl_2(g). This oxidation reduced the chloride surface concentration and favored the CuCl precipitation on the rough CCuPP surface as a chemisorbed monolayer since it disappeared quickly and quasi-simultaneously at any part on the electrode surface. Then, for the last layer we propose this mechanism:

$$2Cl^- \rightarrow Cl_2 + 2e^- \quad (20)$$

$$Cu \rightarrow Cu_{ads}^+ + 1e^- \quad (21)$$

$$Cu_{ads}^+ + Cl^- \rightarrow CuCl_{ads} \quad (22)$$

$$CuCl_{ads} \rightarrow Cu_{aq}^{2+} + Cl^{-} + e^{-} \quad (23)$$

4 CONCLUSIONS

RGB video electrochemistry proved clear as an interesting tool to study and quantify the spatiotemporal color changes of the Cu electrodeposition and electrodissolution on ternary graphite:copper:polypropylene composite in acid media. On the one hand, we can understand the ohmic drop effect during Cu electrodeposition in this kind of resistive electrodes by the analysis of the color changes from the top to the bottom of the electrode independently on the electrode geometry. On the other hand, we can identify possible intermediate species formed on the electrode surface during the Cu electrodissolution. Moreover, we can relate color changes with electrochemical measurements and changes of the electrode surface in contact with the solution.

The time evolution of the standard deviation of the pixel color intensity in the region under study marks singular times where half of the surface color has changed. At this time, the standard deviation shows a peak since the electrode surface changes from one color to another different color. The time at which the peaks appear is related to the ohmic drop effect and in our case with the geometry of the electrode. Both peak symmetry and width peak are related to the color rate growth, or in other words, with the formation or dissolution of different layers on the electrode surface.

We have clearly observed differences between Cu electrodissolution mechanism in aerated H_2SO_4 and HCl aqueous solution. In H_2SO_4, the possible formation of a Cu_2O layer does not represent a protective stable passive layer since the electrodissolution continues suggesting a porous and thin layer. The results suggest that the most of Cu dissolves as Cu(II) species. Therefore, the Cu_2O layer should be formed and after oxidized to soluble Cu(II) species. In HCl solutions, the change of color during the first seconds of electrodissolution also suggests the formation of a thicker Cu_2O layer. In addition, a white-grey layer on the electrode

surface appears at the end of the electrodissolution process attributed to the adsorption-precipitation of CuCl favored by the oxidation of Cl^- to $Cl_2(g)$.

The methodology here presented could be extended for the spatiotemporal study of electrochemical processes on resistive electrodes where electrical current proves non-homogenous on the electrode surface. It could represent an excellent in situ control for the final quality of electroplating processes. For electrodissolution or corrosion processes there is also of special interest coupled with electrochemical techniques for identifying intermediate species. Thus, the RGB video electrochemistry can be considered as a cheap and powerful spectroelectrochemical technique to characterize the electrode surfaces independently of geometry.

ACKNOWLEDGEMENTS

This work was supported by MINECO-FEDER project CTQ2015-71794-R. SEM and EDAX microanalysis was carried out in the Microcopy Section of Central Service for Experimental Research (SCSIE) of the University of Valencia.

REFERENCES

[1] J. Carratalá-Abril, L. Rey-Martínez, R. Beneito-Ruiz, J. Vilaplana-Cerdá, Development of Carbon-based Composite Materials for Energy Storage, Materials Today: Proceedings. 3 (2016) S240–S245. doi:10.1016/j.matpr.2016.02.040.

[2] S. Pande, B. Singh, R. Mathur, T. Dhami, P. Saini, S. Dhawan, Improved Electromagnetic Interference Shielding Properties of MWCNT–PMMA Composites Using Layered Structures, Nanoscale Res Lett. 4 (2009) 327–334. doi:10.1007/s11671-008-9246-x.

[3] J. Agrisuelas, J.J. García-Jareño, P. Rivas, J.M. Rodríguez-Mellado, F. Vicente, Electrochemistry and electrocatalysisof a Pt@poly(neutral red) hybrid nanocomposite, Electrochimica Acta. (n.d.). doi:10.1016/j.electacta.2015.04.120.

[4] H.T. Chung, J.H. Won, P. Zelenay, Active and stable carbon nanotube/nanoparticle composite electrocatalyst for oxygen reduction, Nature Communications. 4 (2013) 1922. doi:10.1038/ncomms2944.

[5] B. Kowalewska, M. Skunik, K. Karnicka, K. Miecmikowski, M. Chojak, G. Ginalska, A. Belcarz, P. Kulesza, Enhancement of bio-electrocatalytic oxygen reduction at the composite film of cobalt porphyrin immobilized within the carbon nanotube-supported peroxidase enzyme, Electrochimica Acta. 53 (2008) 2408–2415. doi:10.1016/j.electacta.2007.10.005.

[6] C. Lau, M.J. Cooney, P. Atanassov, Conductive Macroporous Composite Chitosan−Carbon Nanotube Scaffolds, Langmuir. 24 (2008) 7004–7010. doi:10.1021/la8005597.

[7] J. NavarroLaboulais, J. Trijueque, J.J. GarciaJareno, F. Vicente, Ohmic drop effect on the voltammetric behaviour of graphite plus polyethylene composite electrodes, J. Electroanal. Chem. 422 (1997) 91–97.

[8] M. Rusu, N. Sofian, D. Rusu, Mechanical and thermal properties of zinc powder filled high density polyethylene composites, Polymer Testing. 20 (2001) 409–417. doi:10.1016/S0142-9418(00)00051-9.

[9] J. Navarro-Laboulais, J. Trijueque, J.J. García-Jareño, F. Vicente, Impedance analysis of graphite + polyethylene and graphite + epoxy composite electrodes, Journal of Electroanalytical Chemistry. 399 (1995) 115–120. doi:10.1016/0022-0728(95)04306-3.

[10] L. Beaunier, M. Keddam, J.J. García-Jareño, F. Vicente, J. Navarro-Laboulais, Surface structure determination by SEM image processing and electrochemical impedance of graphite + polyethylene composite electrodes, Journal of Electroanalytical Chemistry. 566 (2004) 159–167. doi:10.1016/j.jelechem.2003.11.022.

[11] J. Gregori, J.J. García-Jareño, F. Negrete, M.P. Peña, C. Sanz, J. Subiela, F. Vicente, Electrochemical dissolution and passivation of nickel powder randomly dispersed in a graphite + polypropylene matrix, Journal of Applied Electrochemistry. 37 (2007) 241–248. doi:10.1007/s10800-006-9247-3.

[12] J. Navarro-Laboulais, J. Trijueque, J.J. García-Jareño, D. Benito, F. Vicente, Determination of the electroactive area of graphite+polyethylene composite electrodes. Uncompensated resistance effects and convolution analysis of chronoamperograms, Journal of Electroanalytical Chemistry. 443 (1998) 41–48. doi:10.1016/S0022-0728(97)00493-2.

[13] J. Trijueque, J.J. García-Jareño, J. Navarro-Laboulais, A. Sanmatías, F. Vicente, Ohmic drop of Prussian-blue/graphite+epoxy electrodes, Electrochimica Acta. 45 (1999) 789–795. doi:10.1016/S0013-4686(99)00257-1.

[14] J. Agrisuelas, J. Garcia-Jareno, M. Piedras, C. Sanz, F. Vicente, Characterization of a New Polypropylene+Graphite+Zinc Ternary Composite, ECS Transactions. 50 (2013) 71–80. doi:10.1149/05050.0071ecst.

[15] A.J. Calandra, N.R. de Tacconi, R. Pereiro, A.J. Arvia, Potentiodynamic current/potential relations for film formation under OHMIC resistance control, Electrochimica Acta. 19 (1974) 901–905. doi:10.1016/0013-4686(74)85041-3.

[16] L. Roullier, E. Laviron, Effect of uncompensated ohmic drop in surface linear potential sweep voltammetry: Application to the determination of surface rate constants, Journal of Electroanalytical Chemistry and Interfacial Electrochemistry. 157 (1983) 193–203. doi:10.1016/S0022-0728(83)80350-7.
[17] S. Gottesfeld, A. Redondo, I. Rubinstein, S.W. Feldberg, Resistance-induced peaks in cyclic voltammograms of systems that can be switched electrochemically between an insulating and conductive state, Journal of Electroanalytical Chemistry and Interfacial Electrochemistry. 265 (1989) 15–22. doi:10.1016/0022-0728(89)80177-9.
[18] J.J. García-Jareño, J. Navarro-Laboulais, F. Vicente, A numerical approach to the voltammograms of the reduction of Prussian blue films on ITO electrodes, Electrochim. Acta. 42 (1997) 1473–1480. doi:10.1016/S0013-4686(96)00302-7.
[19] J.J. García-Jareño, A. Sanmatías, J. Navarro-Laboulais, F. Vicente, Chronoamperometry of prussian blue films on ITO electrodes: ohmic drop and film thickness effect, Electrochimica Acta. 44 (1999) 4753–4762. doi:10.1016/S0013-4686(99)00226-1.
[20] Z. Wang, X. Cai, C. Yang, L. Zhou, Improving strength and high electrical conductivity of multi-walled carbon nanotubes/copper composites fabricated by electrodeposition and powder metallurgy, Journal of Alloys and Compounds. 735 (2018) 905–913. doi:10.1016/j.jallcom.2017.11.200.
[21] P.-M. Hannula, M. Junnila, D. Janas, J. Aromaa, O. Forsén, M. Lundström, Carbon Nanotube Fiber Pretreatments for Electrodeposition of Copper, Advances in Materials Science and Engineering. (2018). doi:10.1155/2018/3071913.
[22] C. Lamy, C. Herrmann, A New Method for Ohmic-Drop Compensation in Potentiostatic Circuits - Stability and Bandpass Analysis, Including Effect of Faradaic Impedance, J. Electroanal. Chem. 59 (1975) 113–135. doi:10.1016/S0022-0728(75)80027-1.
[23] W. Darwich, A. Garron, P. Bockowski, C. Santini, F. Gaillard, P.-H. Haumesser, Impact of surface chemistry on copper deposition in mesoporous silicon, Langmuir. 32 (2016) 7452–7458. doi:10.1021/acs.langmuir.6b00650.
[24] Y. Hori, R. Takahashi, Y. Yoshinami, A. Murata, Electrochemical reduction of CO at a copper electrode, J. Phys. Chem. B. 101 (1997) 7075–7081. doi:10.1021/jp970284i.
[25] T.F. Beltrame, V. Coelho, L. Marder, J.Z. Ferreira, F.A. Marchesini, A.M. Bernardes, Effect of operational parameters and Pd/In catalyst in the reduction of nitrate using copper electrode., Environmental Technology. (2017) 1–13. doi:10.1080/09593330.2017.1367422.
[26] Y.-L. Qiu, H.-X. Zhong, T.-T. Zhang, W.-B. Xu, X.-F. Li, H.-M. Zhang, Copper Electrode Fabricated via Pulse Electrodeposition: Toward High Methane Selectivity and Activity for CO2 Electroreduction, ACS Catal. 7 (2017) 6302–6310. doi:10.1021/acscatal.7b00571.
[27] H. Zhong, K. Fujii, Y. Nakano, Effect of KHCO3 Concentration on Electrochemical Reduction of CO2 on Copper Electrode, J. Electrochem. Soc. 164 (2017) F923–F927. doi:10.1149/2.0601709jes.
[28] T. Hurlen, C. Frengen, N.A. Sörensen, H. Dam, B. Sjöberg, J. Toft, On the Kinetics of the Cu/Cu(aq)++ Electrode., Acta Chemica Scandinavica. 15 (1961) 630–644. doi:10.3891/acta.chem.scand.15-0630.
[29] EQCM-simple-experiment_Ver1_1 - eQCM-Calibration-of-an-Au-coated-Quartz-Crystal-AppNote.pdf, (n.d.). https://www.gamry.com/assets/Uploads/eQCM-Calibration-of-an-Au-coated-Quartz-Crystal-AppNote.pdf (accessed December 18, 2016).
[30] A. Cuenca, J. Agrisuelas, J.J. García-Jareño, F. Vicente, Oscillatory Changes of the Heterogeneous Reactive Layer Detected with the Motional Resistance during the Galvanostatic Deposition of Copper in Sulfuric Solution, Langmuir. 31 (2015) 12664–12673. doi:10.1021/acs.langmuir.5b03694.
[31] A. Cuenca, J. Agrisuelas, R. Catalán, J.J. García-Jareño, F. Vicente, Motional Resistance Evaluation of the Quartz Crystal Microbalance to Study the Formation of a Passive Layer in the

Interfacial Region of a Copper vertical bar Diluted Sulfuric Solution, Langmuir. 31 (2015) 9655–9664. doi:10.1021/acs.langmuir.5b02233.
[32] A. Cuenca, J. Agrisuelas, J.J. García-Jareño, F. Vicente, Alternating current electrogravimetry of copper electrodissolution in a sulfuric acid solution, Electrochimica Acta. 235 (2017) 374–383. doi:10.1016/j.electacta.2017.03.079.
[33] D. Gimenez-Romero, C. Gabrielli, J.J. Garcia-Jareno, H. Perrot, F. Vicente, Electrochemical quartz crystal microbalance study of copper electrochemical reaction in acid medium containing chlorides, J. Electrochem. Soc. 153 (2006) J32–J39.
[34] F.K. Crundwell, The anodic dissolution of copper in hydrochloric acid solutions, Electrochimica Acta. 37 (1992) 2707–2714. doi:10.1016/0013-4686(92)85197-S.
[35] O.E. Barcia, O.R. Mattos, N. Pebere, B. Tribollet, Mass-Transport Study for the Electrodissolution of Copper in 1M Hydrochloric Acid Solution by Impedance, J. Electrochem. Soc. 140 (1993) 2825–2832. doi:10.1149/1.2220917.
[36] C. Deslouis, B. Tribollet, G. Mengoli, M.M. Musiani, Electrochemical behaviour of copper in neutral aerated chloride solution. I. Steady-state investigation, J Appl Electrochem. 18 (1988) 374–383. doi:10.1007/BF01093751.
[37] M.R. Vogt, A. Lachenwitzer, O.M. Magnussen, R.J. Behm, In-situ STM study of the initial stages of corrosion of Cu(100) electrodes in sulfuric and hydrochloric acid solution, Surface Science. 399 (1998) 49–69. doi:10.1016/S0039-6028(97)00811-X.
[38] J. Agrisuelas, J.J. García-Jareño, E. Perianes, F. Vicente, Use of RGB digital video analysis to study electrochemical processes involving color changes, Electrochemistry Communications. 78 (2017) 38–42. doi:10.1016/j.elecom.2017.04.001.
[39] D. Izquierdo, V. Ferraresi-Curotto, A. Heras, R. Pis-Diez, A.C. Gonzalez-Baro, A. Colina, Bidimensional Spectroelectrochemistry: application of a new device in the study of a o-vanillin-copper(II) complex, Electrochimica Acta. 245 (2017) 79–87. doi:10.1016/j.electacta.2017.05.105.
[40] J. Agrisuelas, C. Gabrielli, J.J. Garcia-Jareno, D. Gimenez-Romero, H. Perrot, F. Vicente, Spectroelectrochemical Identification of the Active Sites for Protons and Anions Insertions into Poly-(Azure A) Thin Polymer Films, The Journal of Physical Chemistry C. 111 (2007) 14230–14237. doi:10.1021/jp0741197.
[41] J. Agrisuelas, J.J. García-Jareño, F. Vicente, Identification of Processes Associated with Different Iron Sites in the Prussian Blue Structure by in Situ Electrochemical, Gravimetric, and Spectroscopic Techniques in the dc and ac Regimes, J. Phys. Chem. C. 116 (2012) 1935–1947. doi:10.1021/jp207269c.
[42] J. Agrisuelas, J.J. García-Jareño, F. Vicente, Spatiotemporal colorimetry to reveal electrochemical kinetics of poly(o-toluidine) films along ITO surface, Electrochimica Acta. 269 (2018) 350–358. doi:10.1016/j.electacta.2018.02.157.
[43] S. Elsayed, H. Galal, A. Allam, U. Schmidhalter, Passive reflectance sensing and digital image analysis for assessing quality parameters of mango fruits, Scientia Horticulturae. 212 (2016) 136–147. doi:10.1016/j.scienta.2016.09.046.
[44] E. Hirayama, T. Sugiyama, H. Hisamoto, K. Suzuki, Visual and Colorimetric Lithium Ion Sensing Based on Digital Color Analysis, Anal. Chem. 72 (2000) 465–474. doi:10.1021/ac990588w.
[45] K. Thajee, P. Paengnakorn, W. Wongwilai, K. Grudpan, Application of a webcam camera as a cost-effective sensor with image processing for dual electrochemical – colorimetric detection system, Talanta. 185 (2018) 160–165. doi:10.1016/j.talanta.2018.03.055.
[46] L. Furnell, P.J. Holliman, A. Connell, E.W. Jones, R. Hobbs, C.P. Kershaw, R. Anthony, J. Searle, T. Watson, J. McGettrick, Digital imaging to simultaneously study device lifetimes of multiple dye-sensitized solar cells, Sustain. Energy Fuel. 1 (2017) 362–370. doi:10.1039/C7SE00015D.
[47] M. Vidal, J.M. Amigo, R. Bro, F. van den Berg, M. Ostra, C. Ubide, Image analysis for maintenance of coating quality in nickel electroplating baths – Real time control, Analytica Chimica Acta. 706 (2011) 1–7. doi:10.1016/j.aca.2011.08.007.

[48] J. Agrisuelas, J.J. García-Jareño, F. Vicente, Quantification of electrochromic kinetics by analysis of RGB digital video images, Electrochemistry Communications. 93 (2018) 86–90. doi:10.1016/j.elecom.2018.06.011.
[49] J. Agrisuelas, J.J. García-Jareño, F. Vicente, Evaluating the Practical Use of Digital Video to Study the Effect of Sheet Resistance of Transparent Indium-Tin Oxide Electrodes Using the Galvanostatic Deposition of Poly(o-toluidine), J. Electrochem. Soc. 165 (2018) G101–G107. doi:10.1149/2.1021809jes.
[50] N. Fredj, T.D. Burleigh, Transpassive Dissolution of Copper and Rapid Formation of Brilliant Colored Copper Oxide Films, J. Electrochem. Soc. 158 (2011) C104–C110. doi:10.1149/1.3551525.
[51] S.-H. Jeon, H.-J. Kim, K.-H. Kong, Y.-S. Park, Effects of Copper Addition on the Passivity and Corrosion Behavior of 27Cr-7Ni Hyper Duplex Stainless Steels in Sulfuric Acid Solution, Mater. T. JIM. 56 (2015) 78–84.
[52] T. Tüken, G. Arslan, B. Yazıcı, M. Erbil, The preparation of polypyrrole coated brass and copper electrodes for electrocatalysis, Progress in Organic Coatings. 49 (2004) 153–159. doi:10.1016/j.porgcoat.2003.09.006.
[53] I.L. Soroka, A. Shchukarev, M. Jonsson, N.V. Tarakina, P.A. Korzhavyi, Cuprous hydroxide in a solid form: does it exist?, Dalton Trans. 42 (2013) 9585–9594. doi:10.1039/C3DT50351H.
[54] D. Starosvetsky, N. Sezin, E. Abelev, T. Cohen-Hyams, Y. Ein-Eli, Features of Copper Passivity in Alkaline Solutions at Potentials below Cu2O Formation, J. Electrochem. Soc. 161 (2014) C77–C82. doi:10.1149/2.087401jes.
[55] M.A. Amin, K.F. Khaled, Copper corrosion inhibition in O2-saturated H2SO4 solutions, Corrosion Science. 52 (2010) 1194–1204. doi:10.1016/j.corsci.2009.12.035.
[56] M. Itagaki, T. Mori, K. Watanabe, Channel flow double electrode study on electrochemical oscillation during copper dissolution in acidic chloride solution, Corrosion Science. 41 (1999) 1955–1970. doi:10.1016/S0010-938X(99)00032-3.
[57] K. d. Efird, Potential-pH Diagrams for 90-10 and 70-30 Cu-Ni in Sea Water, CORROSION. 31 (1975) 77–83. doi:10.5006/0010-9312-31.3.77.
[58] B. Trachli, M. Keddam, H. Takenouti, A. Srhiri, Protective effect of electropolymerized 3-amino 1,2,4-triazole towards corrosion of copper in 0.5 M NaCl, Corrosion Science. 44 (2002) 997–1008. doi:10.1016/S0010-938X(01)00124-X.
[59] H.Y.H. Chan, C.G. Takoudis, M.J. Weaver, Oxide Film Formation and Oxygen Adsorption on Copper in Aqueous Media As Probed by Surface-Enhanced Raman Spectroscopy, J. Phys. Chem. B. 103 (1999) 357–365. doi:10.1021/jp983787c.
[60] G. Bech-Nielsen, M. Jaskula, I. Chorkendorff, J. Larsen, The initial behaviour of freshly etched copper in moderately acid, aerated chloride solutions, Electrochimica Acta. 47 (2002) 4279–4290. doi:10.1016/S0013-4686(02)00415-2.
[61] S.N. Ovchinnikova, T.P. Aleksandrova, A.A. Vais, Copper in Acid Chloride Solutions: Electrochemical Behavior by Quartz Microgravimetry and Voltammetry, Russian Journal of Electrochemistry. 40 (2004) 755–759. doi:10.1023/B:RUEL.0000035261.95595.e9.
[62] G. Faita, G. Fiori, D. Salvadore, Copper behaviour in acid and alkaline brines—I kinetics of anodic dissolution in 0.5M NaCl and free-corrosion rates in the presence of oxygen, Corrosion Science. 15 (1975) 383–392. doi:10.1016/0010-938X(75)90005-0.
[63] Handbook of Chemistry and Physics 98th Edition, (n.d.). http://hbcponline.com/faces/documents/04_02/04_02_0047.xhtml (accessed April 10, 2018).

FIGURE LEGENDS

Figure 1. 3D surface contour map of $\bar{I}_G$ against distance from the top of the electrode and the elapsed time during Cu electrodeposition in 0.5 M $CuSO_4$ and 0.1 M H_2SO_4 aqueous solution for (A) 1.1×0.5×0.2 cm^3 short geometry and (B) 2.5×0.5×0.2 cm^3 long geometry. Images show the electrodes before and after Cu electrodeposition.

Figure 2. Covered fraction (θ) profiles (Eq. (9)) during Cu electrodeposition in 0.5 M $CuSO_4$ and 0.1 M H_2SO_4 aqueous solution at different distances for (A) 1.1×0.5×0.2 cm^3 short electrode and (B) 2.5×0.5×0.2 cm^3 long electrode. Numbers on lines show the distance in cm from the top of the electrode. The inset in (A) show the potentiometric results for both geometries. Schema of the three kind of layers obtained during the Cu electrodeposition (below of graphs).

Figure 3. $\bar{I}_G$ (A) and sd_G (B) during the Cu electrodeposition on Pt electrode in 0.5 M $CuSO_4$ and 0.1 M H_2SO_4 aqueous solution

Figure 4. sd_G during the Cu electrodeposition for the short (A) and long (B) electrodes. Numbers on lines show the distance in cm from the top of the electrode. In the inset of A shows $t_{1/2}$ against distance for both geometries.

Figure 5. θ against time obtained at different distance from the top of the electrode and potentiometric results during the Cu electrodissolution in 0.1 M H_2SO_4 aqueous solution for (A) 1.1×0.5×0.2 cm^3 short electrode and (B) 2.5×0.5×0.2 cm^3 long electrode. Numbers on lines indicate distance from the top of the electrode. Electrode images above graphs were extracted from the recorded video at the corresponding time.

Figure 6. sd_R during the Cu electrodissolution for the short (A) and long (B) electrodes in 0.1 M H_2SO_4 aqueous solution. Numbers on lines indicate the distance in cm from the top of the electrode.

Figure 7. $\bar{I}_R$ and E (A) and sd_R (B) during the Cu electrodissolution for the 1.1 cm × 0.5 cm × 0.2 cm short geometry in 0.1 M HCl. Electrode images in (B) were extracted from the recorded video at the corresponding time.

Figure 8. EDAX microanalysis of a CCuPP electrode removed from the solution during the $CuCl_{ads}$ formation. The inset shows the micrograph of the CCuPP electrode surface. SEM images were collected by a Hitachi S-4800 Field Emission Scanning Electron Microscope (SEM) using an acceleration voltage of 20 kV. Green arrow indicates the point at which EDAX microanalysis was done.

FIGURES

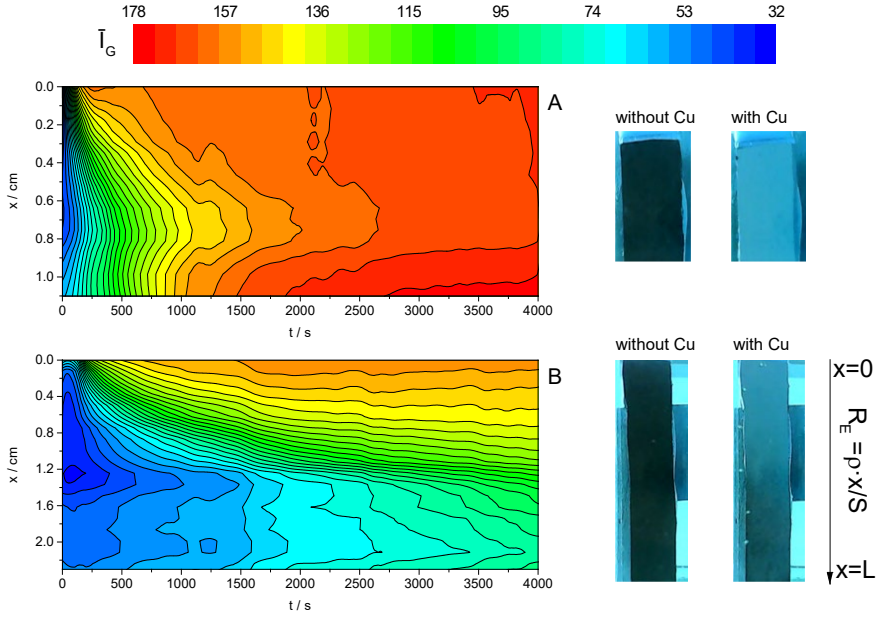

Figure 1

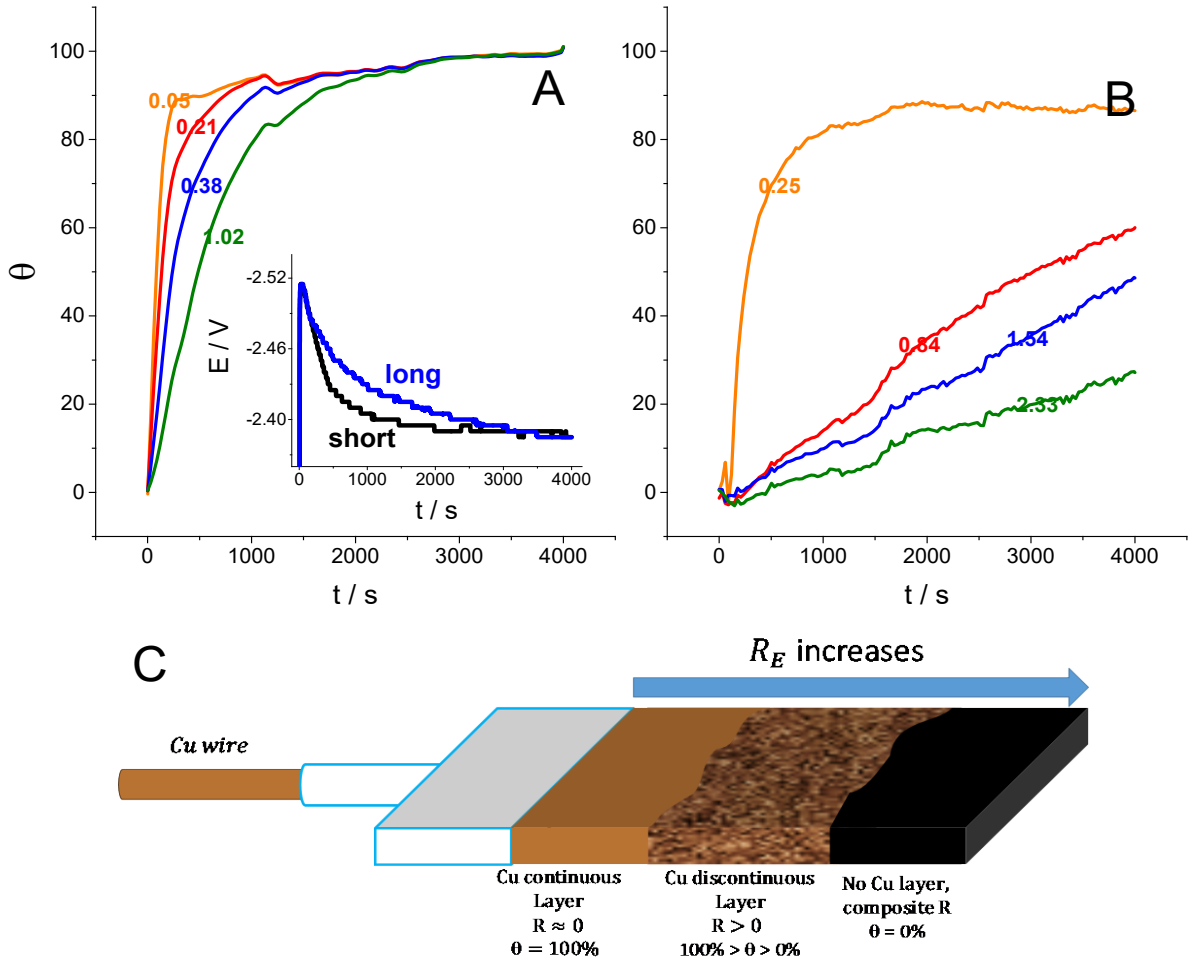
A
B
C
θ
t / s
E / V
0.05
0.21
0.38
1.02
long
short
0.25
0.84
1.34
2.33
R_E increases
Cu wire
Cu continuous Layer
R ≈ 0
θ = 100%
Cu discontinuous Layer
R > 0
100% > θ > 0%
No Cu layer, composite R
θ = 0%

Figure 2

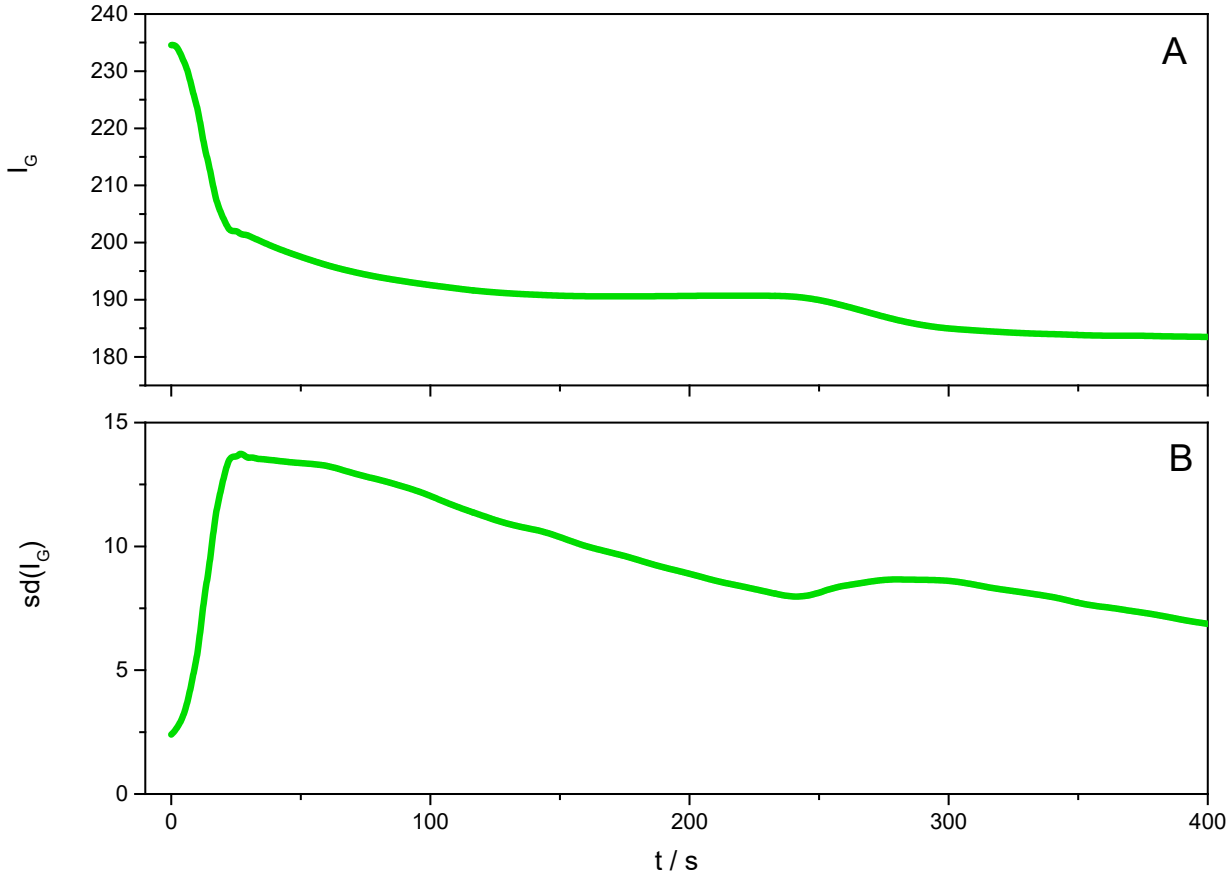
A
B
I_G
$sd(I_G)$
t / s
240
230
220
210
200
190
180
15
10
5
0
0
100
200
300
400

Figure 3

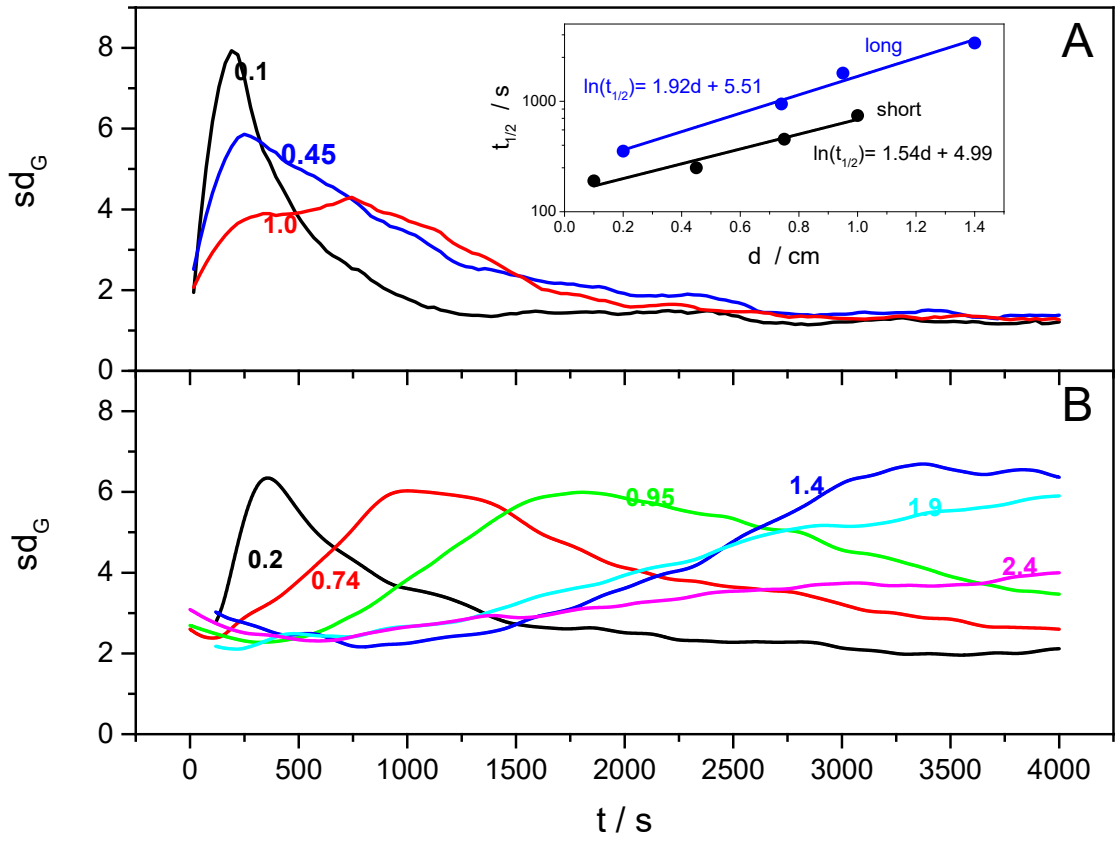
A
B
sd_G
sd_G
0.1
0.45
1.0
0.2
0.74
0.95
1.4
1.9
2.4
long
short
ln(t_1/2)= 1.92d + 5.51
ln(t_1/2)= 1.54d + 4.99
t_1/2 / s
d / cm
t / s

Figure 4

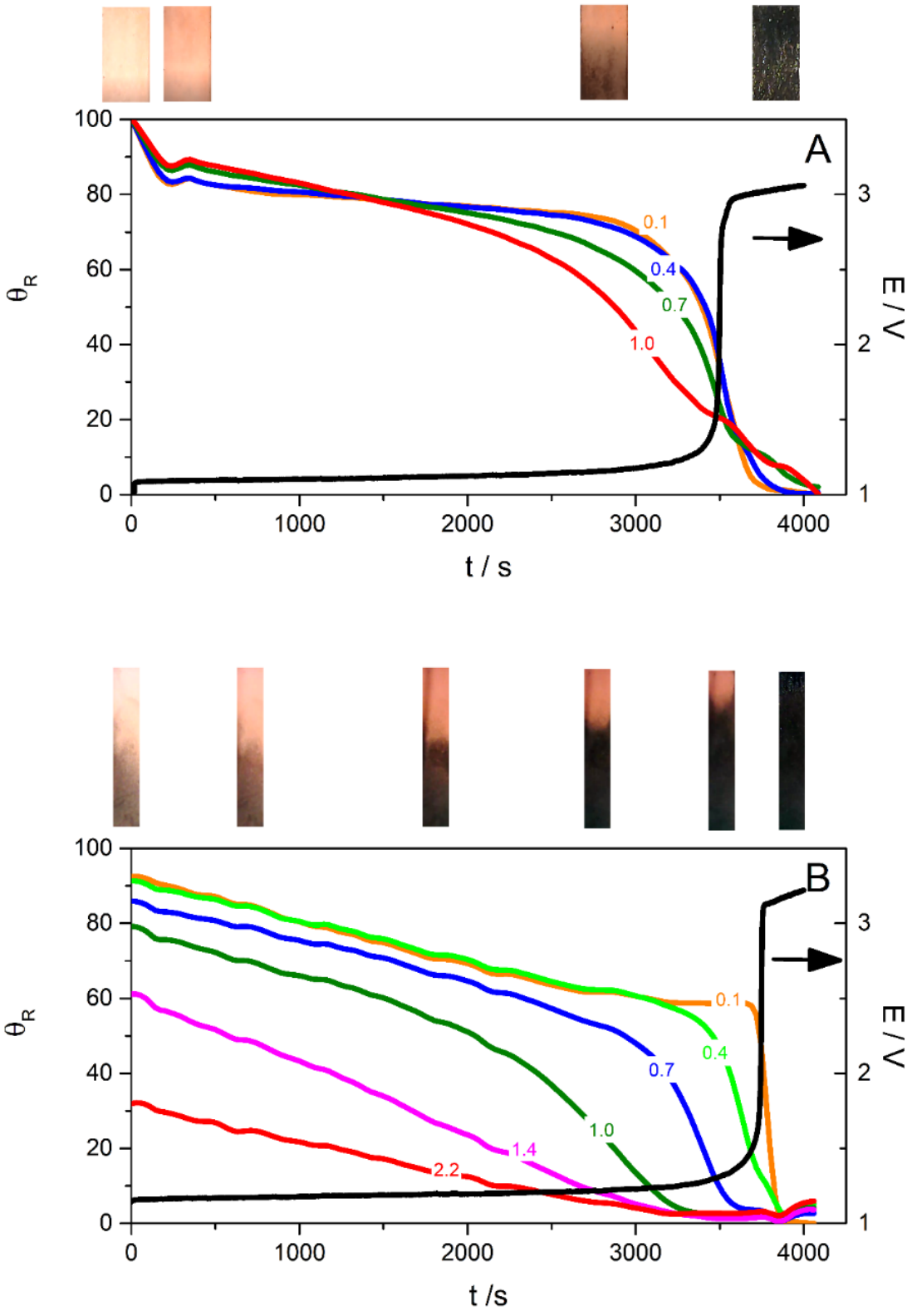
A
B
θR
E / V
t / s
t /s
0.1
0.4
0.7
1.0
1.4
2.2
0
20
40
60
80
100
1
2
3
0
1000
2000
3000
4000

Figure 5

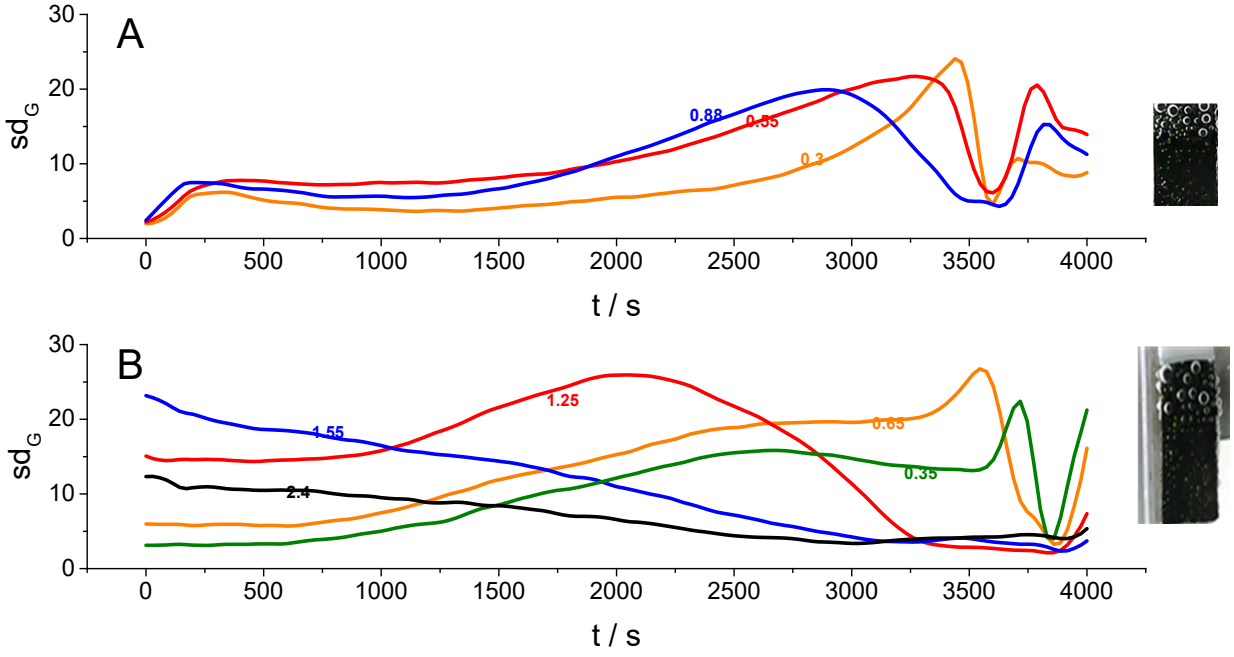

Figure 6

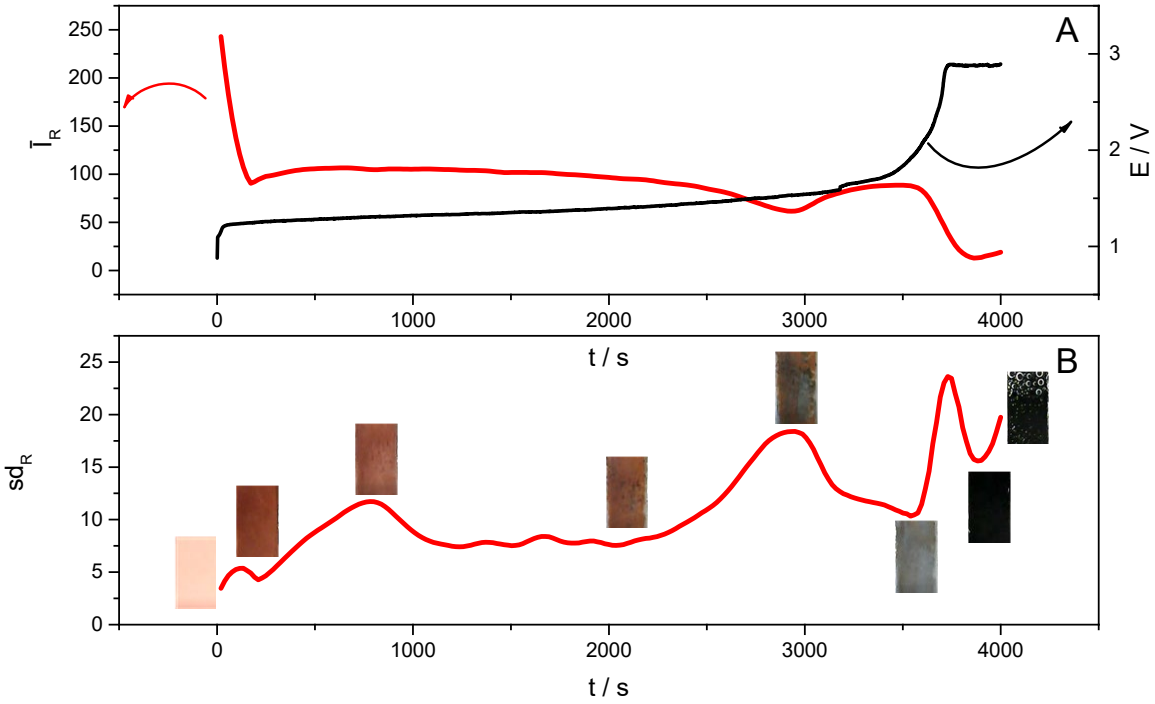
A
B
$\bar{I}_R$
E / V
sd_R
t / s
t / s
0
50
100
150
200
250
1
2
3
0
5
10
15
20
25
0
1000
2000
3000
4000

Figure 7

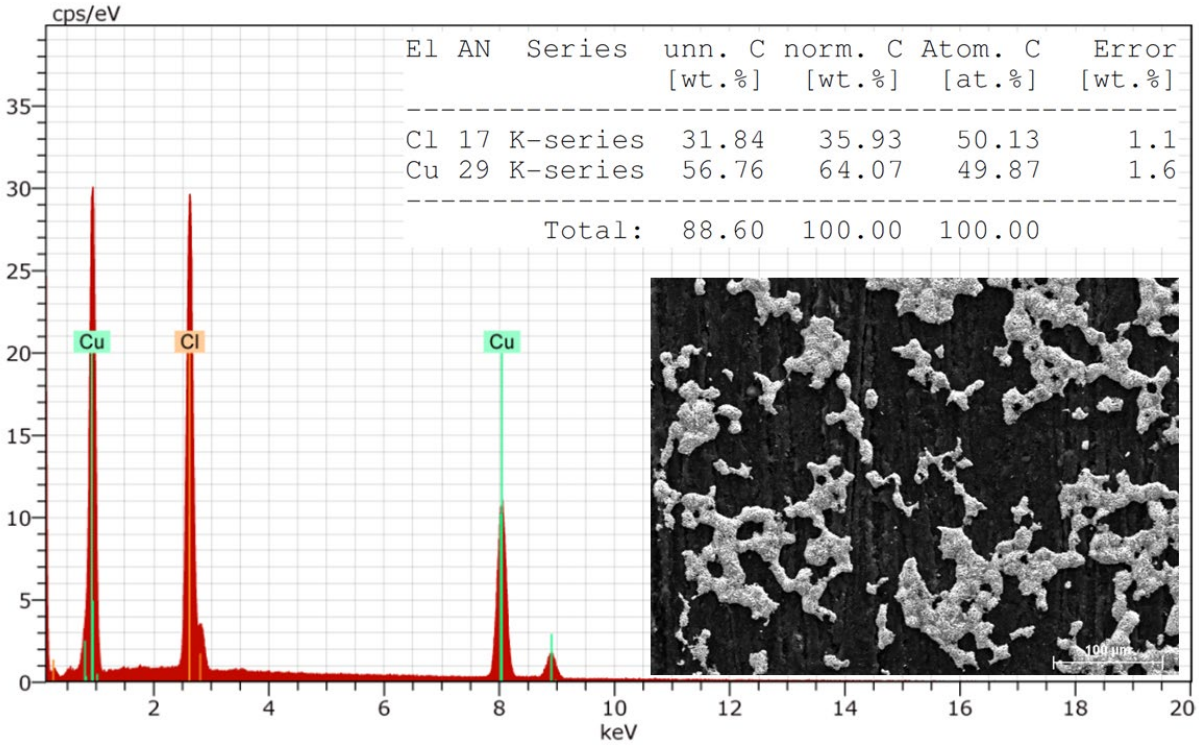
cps/eV
El AN Series unn. C [wt.%] norm. C [wt.%] Atom. C [at.%] Error [wt.%]
Cl 17 K-series 31.84 35.93 50.13 1.1
Cu 29 K-series 56.76 64.07 49.87 1.6
Total: 88.60 100.00 100.00
Cu
Cl
Cu
100 µm
keV

Figure 8